WILEY | Hindawi

Research Article

Key Technologies of Steel Plate Surface Defect Detection System Based on Artificial Intelligence Machine Vision

Bin Xue[1,2] **and Zhisheng Wu** [1]

[1]*School of Materials Science and Engineering, Taiyuan University of Science and Technology, Taiyuan, 030024 Shanxi, China*
[2]*School of Mechanical and Electrical Engineering, Qingdao Binhai University, Qingdao 266555, Shandong, China*

Correspondence should be addressed to Zhisheng Wu; zswu1963@tyust.edu.cn

With the rapid development of visual inspection technology, computer technology, and image processing technology, machine vision technology has become more and more mature, and the role of quality inspection and control in the steel industry is becoming more and more obvious and important. Defects on the surface of the strip are a key factor affecting the quality inspection process. Its inspection plays an extremely important role in improving the final quality. For a long time, traditional manual inspection methods cannot meet actual production needs, so in-depth research on steel surface defect inspection systems has become the consensus of today's steel companies. The accuracy and low performance of traditional detection methods can no longer meet the needs of people and society. The surface defect detection method based on machine vision has the characteristics of high accuracy, fast processing speed, and intelligent processing, which is the main trend of surface defect detection. We select a steel plate; take the invariant moment features of the cracks, holes, scratches, oil stains, and other images on it; extract the data results; and analyze them. Then, we read the texture features of these defect images again, extract the data results, and analyze them. The experimental results prove that after the mean value filter and Gaussian filter process the image, the mean variance value MSE is relatively large (46.276 > 31.2271), and as the concentration of salt and pepper noise increases, the rate of increase of MSE increases obviously, and as the peak signal-to-noise ratio and the mean variance value MSE increase continuously (32.2271 < 33.3695), the image distortion is more serious. The method designed in this paper is extremely effective. Improving the surface quality of steel is of great significance to improving market competitiveness.

1. Introduction

Ophthalmic diseases have more complex causes, more different diseases, and more variable conditions and belong to clinical ophthalmic diseases [1]. It will seriously affect the vision of the patient and may even cause blindness. Therefore, in order to effectively improve the vision of patients, the above-mentioned various consequences must be effectively prevented. Due to the introduction of advanced technology and production technology, product quality and standard production technology have been significantly improved in recent decades. However, due to the extensive influence of many complex reasons, such as initial production habits and inspection methods, it is used as steel. A large part of the surface quality has not changed much. As an important raw material for modernization [2], steel plates are used in all aspects of social development, from bridge construction to aerospace machinery and many other essential fields. The quality of the metal plate is directly related to the reliability of public use and the safety of society and public industries [3]. Detecting and inspecting the surface defects of steel plates are currently the primary task of steel companies. The development of a cost-effective surface quality inspection system suitable for Chinese steel companies has become a top priority.

Defects on the surface of the strip are a key indicator for evaluating the quality of the film. The effective method of detecting defects has attracted people's attention for a long time. Researchers at home and abroad have done a lot of work for this and achieved some results. Ohkubo et al.
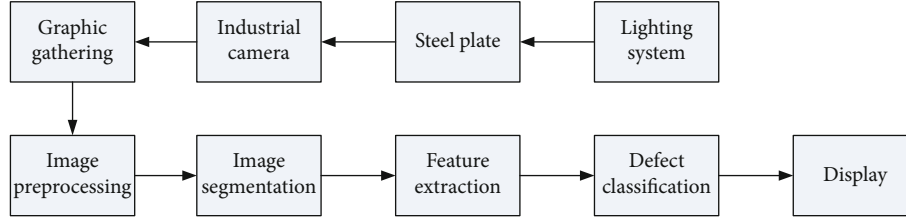
FIGURE 1: System flow chart.

proposed a detection system that uses a laser as a scanning light source, a 12-sided reflective prism and a cylindrical mirror as an optical system, and a photomultiplier tube to receive the detection system [4, 5]. Liu et al. proposed the theory of eddy current testing and successfully used eddy current testing technology to detect metal barium, which opened up the research boom of eddy current testing in the application of metal surface defect detection [6]. Choudhary et al. have developed an online automatic detection system for surface defects of continuous casting billets, which has set off a research boom in infrared detection of surface defects [7]. Dombrowski et al. chose a fully programmable image digitizer and a fully programmable high-speed digital signal processor to process digital image signals and used the system for cold-rolled strip steel surface, edge cracks, and other edge tests [8]. Shu et al. conducted the research on the strip steel surface detection system which analyzes the CCD detection method and proposes some effective algorithms [9]. Hossam et al. use computer image processing technology and pattern recognition technology to perform image processing and defect classification algorithms and perform effective surface defect detection [10]. Therefore, the research on the key technology of the steel plate surface defect detection system based on artificial intelligence machine vision is of great significance.

The existing extraction methods are mainly aimed at normal retinal images, which are not universal; this paper adopts an improved maximum classification algorithm based on constant torque to solve the inefficient ground-to-ground detection problem, using gray scale and texture feature extraction methods, feature selection methods based on principal component analysis, and defect classification algorithms based on support carrier machines. Research on key technologies such as image processing and detection system classification and recognition has solved the problem of steel surface defect detection system. Defect segmentation takes a long time, there are many feature sizes, and the classification result is low.

2. Key Technologies of Steel Plate Surface Defect Detection System Based on Artificial Intelligence Machine Vision

2.1. Defect Image Preprocessing and Segmentation Technology

2.1.1. Image Denoising Analysis. Generally, we hope that the image captured by the camera is clear and noise-free [11]. Since optoelectronic noise will hinder the conversion of images from optical to electronic forms and electronic signal

TABLE 1: Summary table of reliability test results.

Category	Index combination	Alpha coefficient (α)
Crack	The crack itself	0.8227
	Crack right	
	Crack left	
	Crack transpose	
Hole	The hole itself	0.8742
	Hole moves right	
	Hole moves left	
	Hole transposition	
Bruise	Bruise itself	0.7663
	Bruise shifts right	
	Bruise shifts left	
	Bruise transposition	
Inclusion	Inclusion itself	0.7414
	Inclusion shifts right	
	Inclusion shifts left	
	Inclusion transposition	

processing amplifiers will cause thermal noise interference, images will inevitably produce noise during this series of complex processing processes [12, 13]. After that, the method of comparative treatment was adopted, and the experimental group and the control group were compared with two different treatment methods. According to the relationship between noise and signal, it can be divided into additional noise and amplified noise [14].

(1) Types of Noise. The probability density function obeys a kind of noise with Gaussian distribution, and the one-dimensional probability density function is shown in the following formula:

$$P(x) = \frac{1}{\sqrt{2\prod}} \exp\left[-\frac{(x-\mu)^2}{2\sigma^2}\right]. \tag{1}$$

Among them, x is the gray value, μ is the mean value, and σ^2 is the variance. Suppose a useful signal is $f(x, y)$ and noise is $m(x, y)$ and the output signal is $g(x, y)$ under the influence of the noise signal, then

$$g(x, y) = f(x, y) + n(x, y) = f(x, y) + \mu + \sigma X. \tag{2}$$

TABLE 2: Invariant moment feature extraction data table.

| Sample defect type	IM1	IM2	IM3	IM4	IM5	IM6	IM7
The crack itself	3.9843	17.7438	7.6313	2.6201	4.3140	5.4762	12.6321
Crack right	3.3242	10.8950	7.3796	2.3861	4.6513	1.3793	7.2141
Crack left	3.5124	11.3472	9.3724	2.3912	2.6724	1.6742	6.3241
Crack transpose	3.9843	17.7438	9.1313	2.1201	3.8140	0.4762	12.6321
The hole itself	5.7260	31.5000	27.8151	27.1595	15.6138	19.4741	9.6081
Hole moves right	5.7260	31.5000	27.8151	27.1595	15.6138	19.4741	9.6081
Hole moves left	5.7260	31.5000	27.8151	27.1595	15.6138	19.4741	9.6081
Hole transposition	5.7260	31.5000	27.8151	27.1595	15.6138	0.8770	9.6081
Bruise itself	2.7234	4.7278	7.5965	6.4868	8.2521	9.7417	9.6433
Bruise shifts right	2.5343	2.9342	1.2417	7.5237	3.8921	5.8660	5.4276
Bruise shifts left	2.5621	3.1137	1.2887	45181	2.7710	2.7770	0.3873
Bruise transposition	2.7234	4.7278	0.5965	2.4868	0.2521	2.7417	0.6433
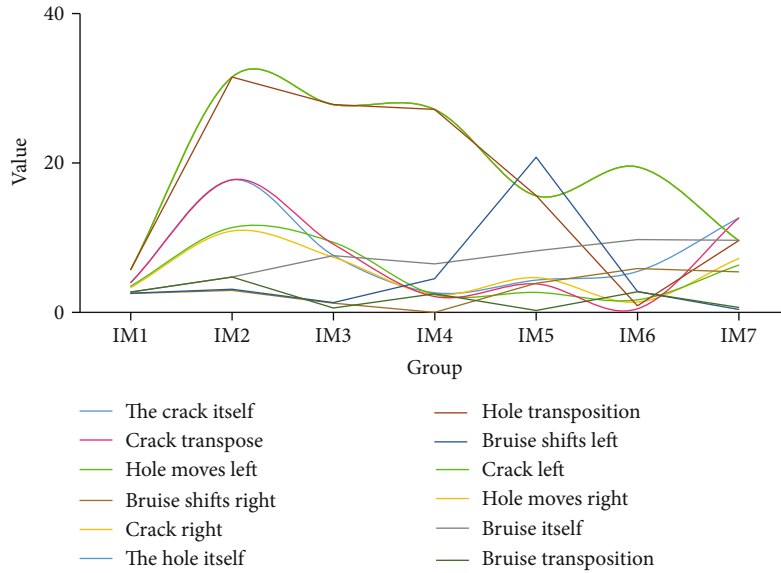
FIGURE 2: Moment invariant feature extraction data analysis diagram.

In multiplicative noise, the relationship is as follows:

$$g(x, y) = f(x, y)[1 + n(x, y)] = f(x, y) + f(x, y)n(x, y). \quad (3)$$

Some infection spots with small gray values (close to black) or large gray values (close to white) appear in the image, and dark and bright spots similar to pepper and salt particles appear in the image, calculated as follows:

$$g(x, y) = \begin{cases} 0, & f(x, y) < \dfrac{2}{d}, \\ 255, & \dfrac{2}{d} \leq f(x, y) \leq d, \\ f(x, y), & \text{otherwise.} \end{cases} \quad (4)$$

(2) Mean Filter. The filtering process of the mean is to make the window slide in the image, then find the average value of each pixel in its neighborhood, and finally replace the value of the center position of the window with the average value of each point in the window [15–17]. Assuming an image $f(x, y)$ of $n \times n$, an image $g(x, y)$ is obtained after the mean filtering process is as shown in the following equation:

$$g(x, y) = \frac{1}{M} \sum_{(m,n) \in S} f(x - m, y - n). \quad (5)$$

In the formula, S is the predetermined neighborhood and M is the total number of pixels contained in the neighborhood. The gray value of each pixel in the image $g(x, y)$ is determined by the average value of the gray values of several pixels of $f(x, y)$ contained in the predetermined neighborhood of (x, y). The area with a radius of 1 is expressed as

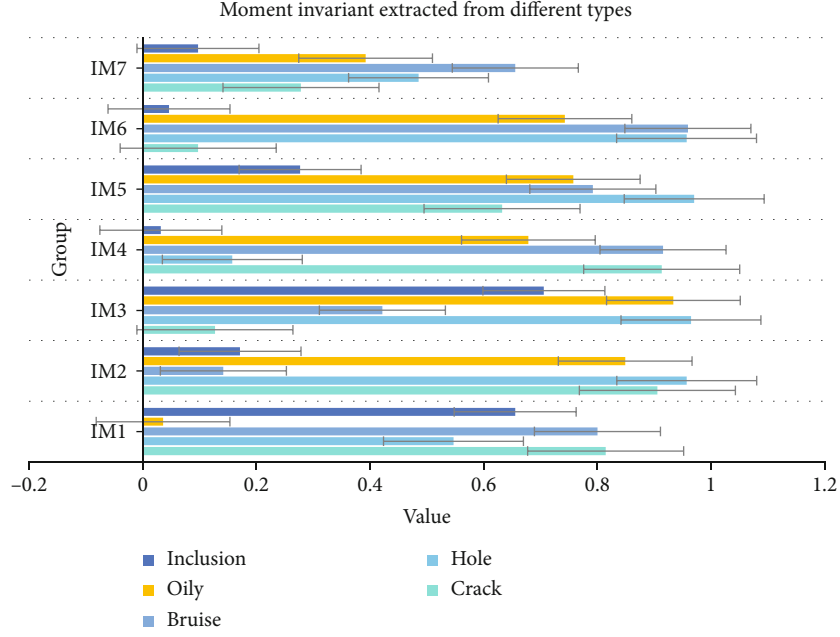$$S_1 = \{(x, y + 1), (x, y - 1), (x + 1, y), (x - 1, y)\}. \quad (6)$$

Moment invariant extracted from different types

Figure 3: Moment invariant feature maps extracted from different types of defects.

Table 3: Defect image texture feature extraction table.

Defect sample	Crack	Hole	Bruise	Oily	Inclusion
Energy	0.9547	0.9491	0.8798	0.9736	0.8473
Mean gray value	0.0278	0.0121	0.0372	0.0232	0.1422
Gray mean square error	0.3312	0.0378	0.6208	0.3564	1.0381
Gradient mean	0.1639	0.0761	0.3942	0.1536	0.2010
Gradient mean square error	2.6790	0.9712	4.0097	2.7180	4.9014
Gray entropy	0.0540	0.0166	0.0719	0.0794	0.0359
Gradient entropy	0.0534	0.0154	0.0565	0.0670	0.1673
Mixed entropy	0.0796	0.0165	0.1185	0.1786	0.1451

Formula (5) is expressed by convolution.

$$g(x, y) = h(x, y) * f(x, y) = \sum_{(m,n) \in S} \sum h(m, n) f(x - m, y - n). \tag{7}$$

(3) Wiener Filter. Wiener filtering is an adaptive filter that minimizes the average square error between the original image and the restored image. The smaller the mean square error, the better the filtering effect of filtering noise [18, 19]. The mean and variance are

$$\mu = \frac{1}{MN} \sum_{(i,j) \in S} F(i, j),$$

$$\sigma^2 = \frac{1}{MN} \sum_{(i,j) \in S} F^2(i, j). \tag{8}$$

In the formula, S is the $M \times N$ field of each pixel, and its estimated formula is

$$G[i, j] = \mu + \frac{\sigma^2 - \nu^2}{\sigma^2} [F(i, j) - \mu]. \tag{9}$$

In nanomaterials, when the particle size reaches a certain physical characteristic size, the energy levels of electrons adjacent to the metal Fermi plane change from an almost continuous state to a discrete state, while the nanoparticles have discontinuous, higher-occupancy molecules.

2.1.2. Filter Effect Evaluation and Result Analysis. After filtering the image, we must also evaluate the image quality [20]. Image quality mainly includes two aspects: one is the degree of difference between the image and the original standard image; the other is the ability of the image to provide information to individuals or machines from subjective and

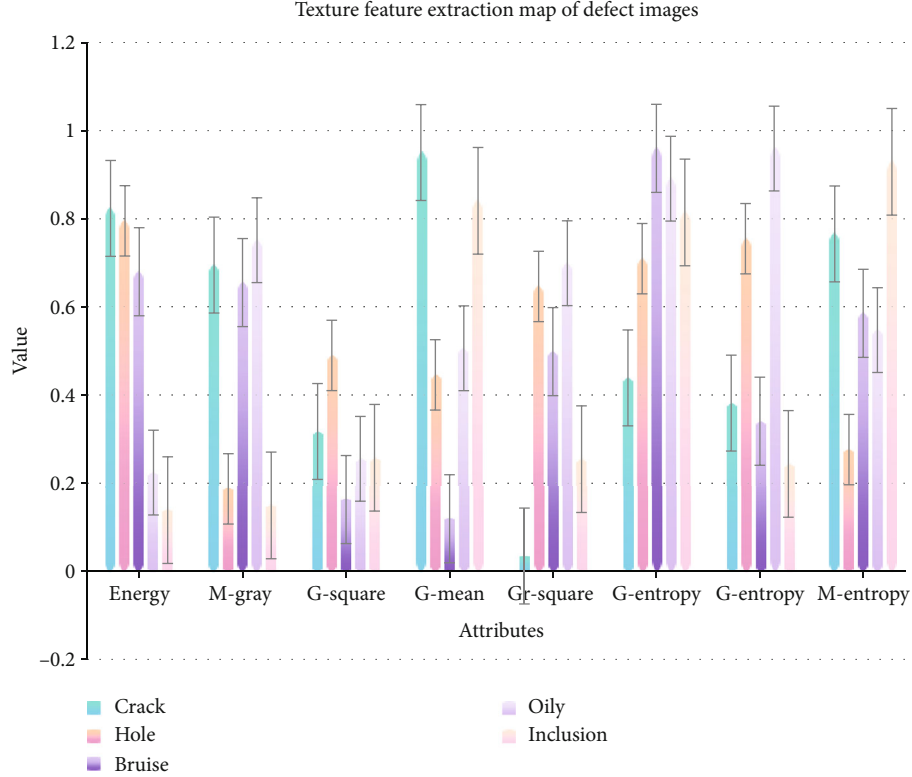Texture feature extraction map of defect images

FIGURE 4: Texture feature extraction map of defect images.

objective aspects. Commonly used indicators are the signal-to-noise ratio of PSNR and the normalized mean square error NMSE [21, 22]. They are expressed as follows:

$$\text{PSNR} = 10 \log \frac{255^2}{1/MN \sum_{j=0}^{M-1} \sum_{i=0}^{N-1} \left(f_{ij} - e_{ij} \right)^2},$$

$$\text{NMSE} = \sum_{i=1}^{N} \sum_{j=1}^{N} \frac{\left| f(i,j) - f'(i,j) \right|^2}{f(i,j)^2}. \tag{10}$$

2.1.3. Two-Dimensional Maximum Entropy Threshold.
Assuming that the A region and the B region have different probability distributions, the posterior probability p_{ij} of the A region and the B region is used to normalize the probability of each region to make the partition entropy have additivity, and the threshold is set at (s, t), then

$$H = -\sum_{i=0}^{L=1} \sum_{j=0}^{L=1} p_{ij} \ln p_{ij}. \tag{11}$$

Then, the two-dimensional entropy of zone A and zone B is

$$H(A) = -\sum_{i=0}^{s} \sum_{j=0}^{t} \left(\frac{p_{ij}}{p_A} \right) \ln \left(\frac{p_{ij}}{p_A} \right) = \ln p_A + \frac{H_A}{p_A},$$

$$H(B) = -\sum_{i=s+1}^{L=1} \sum_{j=t+1}^{L=1} \left(\frac{p_{ij}}{p_B} \right) \ln \left(\frac{p_{ij}}{p_B} \right) = \ln p_B + \frac{H_B}{p_B}. \tag{12}$$

The discriminant function that defines entropy is

$$\phi(s, t) = H_{(A)} + H_{(B)}. \tag{13}$$

2.2. Traditional Threshold Segmentation Technology.
The so-called threshold segmentation technology is to use a threshold in the picture to divide the entire picture into two parts, a black part and a white part, with one part as the target object and the other part as the background object [23–25]. Throughout the scientific frontier literature and books on nanoelectrocatalysts, the most mentioned word is energy. Energy is no longer a problem of a certain country but has become a problem of global concern. When a crisis occurs, there is no one. The country can take care of itself. The vast number of scientific researchers is working against clean energy. Based on Otsu threshold segmentation, an iterative threshold segmentation was proposed.

2.2.1. Otsu Threshold Segmentation Method.
In the process of detecting data image defects, if you want to request the

TABLE 4: Depression data analysis table.

Sample number	$\bar{m}$	σ^2	m_η	m_k	E	H
1	-0.6666	-0.6961	0.2436	1.9268	-0.3848	-0.5962
2	-0.7104	-0.7108	0.5538	1.7370	-0.3880	-0.6295
3	-0.6335	-0.6378	0.4459	1.8837	-0.3642	-0.6141
4	-0.8493	-0.8457	1.3670	0.9165	0.1147	-0.7533
5	-0.7154	-0.7567	0.8430	1.6722	-0.2849	-0.6791
6	-0.7378	-0.7761	0.6645	1.7827	-0.2274	-0.6609
7	-0.5272	-0.5786	0.1737	1.9857	-0.4264	-0.5432
8	-0.7264	-0.7565	0.7528	1.6483	-0.2781	-0.6341
9	-0.8715	-0.8262	0.9458	1.4934	-0.1535	-0.6670

FIGURE 5: Standardized processing diagram of feature data.

optimal threshold, you must cross all pixel values in the gray-scale range and calculate the amount of change. When the amount of calculation is large, the output will be very low [26, 27]. At the same time, due to the influence of factors such as the gray level of the image itself and the noise interference that has not been eliminated, the best limit cannot be reached by using only the gray histogram, which will lead to very unsatisfactory processing results [28].

2.2.2. Iterative Threshold Segmentation Method. Compared with the Otsu threshold segmentation, it is not necessary to determine an optimal threshold for each picture, which has a certain degree of adaptability [29, 30]. The specific steps are as follows. First, determine a parameter T0 based on pictures and experience, and select a preliminary estimated threshold T1. Then, use T1 to divide the image into two parts.

2.3. Improved Threshold Segmentation Algorithm Based on Pixel Search. In the detection process of steel plate surface defects [31], some defects occupy fewer pixels and have a low signal-to-noise ratio. Due to the reflective characteristics of the steel plate surface, the background light is uneven, and the defect characteristics and the background gray value are not obvious. After the research of the previous section, it is found that the processing effect of traditional edge detection and threshold segmentation algorithms is not ideal [29, 32]. In order to improve the segmentation of weak steel plate surface defect features, this section explores the use of pixel search methods. Defect threshold segmentation is carried out, and the method of segmentation of weak defect images is combined in the segmentation process. As a result, it is found that the segmentation effect has certain advantages, which is of great help to the later feature extraction of steel plate defects [33].

Integrate the various small areas so that the steel plate defect target and background can be separated as a whole [34, 35]. Uveitis is a chronic inflammation. At present, gluco-corticoids, nonsteroidal anti-inflammatory drugs, and immunosuppressive agents can effectively treat uveitis, but these drugs have difficulty reaching the retina to achieve a complete therapeutic effect. Therefore, treating uveitis remains a challenge. Recent studies have shown that nanocells can improve the solubility of drugs and increase the per-
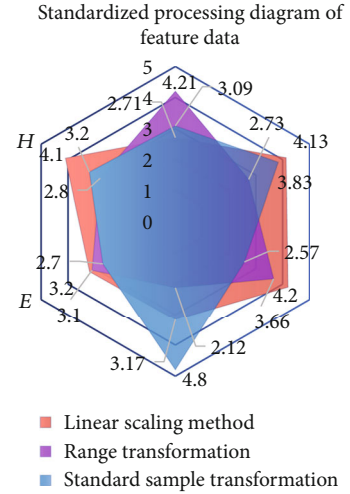
meability of conjunctival epithelial cells through good hydrophilicity and high drug encapsulation potential. Finally, each defect target will not exist in the form of a pixel, and it must meet the gray level of the same area. Uniformity and connectivity must be achieved, so that the segmented defect images can better meet the needs of defect feature extraction.

In view of the small defect segmentation problem where the contrast between the defect target and the background is not obvious due to uneven illumination of the steel plate surface image and the reflection of the steel plate itself, the steel plate defect target segmentation algorithm proposed in this section fully considers the similarity of the defect target and the background pixel in the same area. Therefore, in the process of target segmentation, first, divide a small area; then, discharge whether there are defective targets in the small area; and finally, confirm whether the small defective target is a target [36, 37]. The specific implementation process of the target segmentation algorithm based on pixel search in the entire segmentation process is as follows:

(1) The preprocessed steel plate surface image is divided into different small areas. In the small areas, each small area can be a background image or a combination of a background image and a defect target. It is better not to be all defective images

(2) Calculate the variance of each small area, and arrange them in an ordered sequence in the order of variance

(3) Set an initial threshold. If the variance change range is less than the initial threshold, the small area is determined to be a background image; if the variance change range is greater than the initial threshold, the small area is determined to have a defective target

(4) If it is determined that there is a defective target in a small area, the threshold within the variance is determined adaptively; if it is greater than the threshold within the variance, it is determined as the defective

TABLE 5: Analysis table based on the experimental results of image denoising.

Assignment variable		Proportion
Mean filter	No salt and pepper added	93.33%
	15% salt and pepper	
	30% salt and pepper	
	50% salt and pepper	
Gaussian filtering	No salt and pepper added	94.44%
	15% salt and pepper	
	30% salt and pepper	
	50% salt and pepper	
Median filter	No salt and pepper added	91.43%
	15% salt and pepper	
	30% salt and pepper	
	50% salt and pepper	
Median filtering based on partial differentiation	No salt and pepper added	94.12%
	15% salt and pepper	
	30% salt and pepper	
	50% salt and pepper	

target; and if it is less than the threshold within the variance, it is determined as the background image

(5) After traversing each small area, each small area is divided into two parts: the defect target and the background. During the whole process, some backgrounds will be mistaken for the surface defect target of the steel plate, so it must be eliminated. The defect target has a certain path. Connected domains exist. This article takes the current pixel as the center and sets a $3 * 3$ window. If more than half of the pixels in this window are defective pixels, it is confirmed that the pixel is a defective point

3. Key Technologies of Steel Plate Surface Defect Inspection System

3.1. System Composition. The steel plate surface defect detection system based on machine vision is mainly composed of optical lighting system, industrial camera, image acquisition system, image processing system, terminal computer, and data management system [38]. The system consists of two parts: hardware system and software system. The system flow chart is shown as in Figure 1.

3.2. Test Subject. The three doctors with rich work experience in this hospital are comprehensively judged for judging the degree of treatment. If there is a dispute, the result can be selected through discussion. We can regard the gray level of an image as a two-dimensional gray density function; then, a gray matrix can be used to describe the image moment features. We select a steel plate; take the invariant moment features of the cracks, holes, scratches, oil stains, and other images on it; extract the data results; and analyze them. Then, we read the texture features of these defect images again,

extract the data results, and analyze them. Taking the image of steel plate without bonding defects and adding different concentrations of salt and pepper noise as the research object, 4 kinds of filtering methods are used to denoise mixed experiments.

3.3. Experimental Method. There are many ways of data standard processing, but different data standardization methods will have a certain impact on the evaluation results of the system. For the positive index standardization method,

$$y_{ij} = \frac{x_{ij} - \min\{x_{ij}\}}{\max\{x_{ij}\} - \min\{x_{ij}\}}. \tag{14}$$

For the negative index standardization method,

$$y_{ij} = \frac{\max\{x_{ij}\} - x_{ij}}{\max\{x_{ij}\} - \min\{x_{ij}\}}. \tag{15}$$

After standardizing the data, using the principal component analysis of nonlinear logarithmic centering, the processing steps of logarithmic transformation and row vector centering are

$$z_{ij} = \ln y_{ij} - \frac{\sum_{i=1}^{m} \ln y_{ij}}{m}. \tag{16}$$

3.4. Statistical Data Processing Method. SPSS23.0 software was used for data processing, and the count data was expressed as a percentage (%), k is the number of data in this experiment, σ^2 is the variance of all survey results, and $P < 0.05$ indicates that the difference is statistically significant. The formula for calculating reliability is shown in the following equation:

$$a = \frac{k}{k-1} \left(1 - \frac{\sum \sigma_i^2}{\sigma^2} \right). \tag{17}$$

4. Key Technology Research on Steel Plate Surface Defect Detection System

4.1. Evaluation Index System Based on Index Reliability Testing. Reliability refers to the stability and reliability of the questionnaire [39]. This article adopts the α coefficient method created by L.J. Cronbach. The α coefficient can be obtained by Reliability Analysis in SPSS software. It is generally believed that the α coefficient above 0.8 indicates that the effect of the index setting is very good, and above 0.7 is also acceptable. Here, we analyze the reliability of each type of object, and the reliability index we choose for each type of object is slightly different. The results are shown in Table 1.

It can be seen from Table 1 that the data obtained from the surface defects of various steel plates has an acceptable influence on this experiment ($\alpha > 0.7$), and the influence of the data around the defects on the surface of various steel plates is acceptable. Within the scope, meet the prerequisites for the start of the experiment.
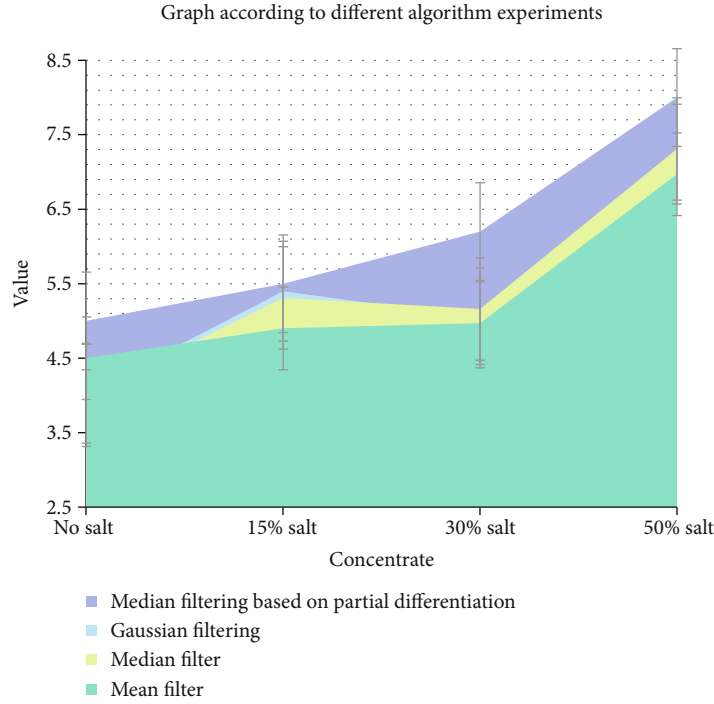
Graph according to different algorithm experiments

FIGURE 6: Analyze the graph according to different algorithm experiments.

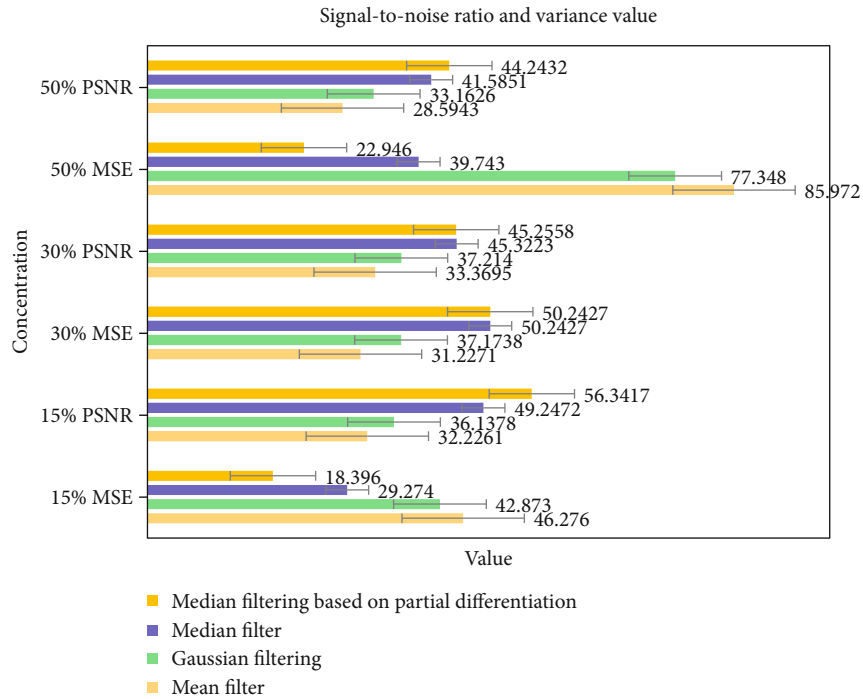Signal-to-noise ratio and variance value

FIGURE 7: Analyze the graph according to the signal-to-noise ratio and variance value.

4.2. Sample Feature Extraction Data Analysis

4.2.1. Invariant Moment Feature Extraction Data Analysis.
Feature extraction, as a key link in the image processing process in the system, is an important process to ensure the practicability of the system and the accuracy of defect recognition

[38]. We separately analyze the cracks, holes, scratches, and inclusion defects in the samples and their own, right shift. The left-shifted and transposed image extracts moment-invariant features. The extraction results are shown in Table 2. We make a line graph based on this result, as shown in Figure 2.

TABLE 6: Analysis table based on the experimental results of image denoising.

Filtering algorithm	15% salt and pepper noise		30% salt and pepper noise		50% salt and pepper noise	
	MSE	PSNR	MSE	PSNR	MSE	PSNR
Mean filter	46.276	32. 2271	31. 2271	33.3695	85.972	28. 5943
Gaussian filtering	42.873	36.1378	37.1738	37.2514	77.348	33. 1626
Median filter	29.274	49.2472	50.2427	45.3223	39.734	41.5851
Median filtering based on partial differentiation	18.396	56. 3471	57. 4317	45.2558	22.946	44.2432.

It can be seen from Figure 2 that the invariant moments of the same type of defects are not much different after they are themselves shifted left, shifted right, or transposed. The two groups of patients were compared at the end of the first course of treatment and at the end of the second course of treatment. The anxiety level of the experimental group is lower than that of the control group during half of the treatment. This conclusion is reliable, and there is no significant difference.

Feature extraction, as a key link in the image processing process in the system, is an important process to ensure the practicability of the system and the accuracy of defect recognition. We gather the moment invariant features extracted from different types of defects according to Table 2, and the results are shown in Figure 3.

It can be seen from Figure 3 that the invariant moments of different types of defects themselves, after shifting to the left, shifting right, or rotating, are quite different, which also verifies that the invariant moments have translation and rotation invariance. This also proves the accuracy of the median filtering algorithm system based on partial differentiation selected in this paper from the side. The new gray median value obtained by the algorithm can more accurately restore the original pixel value when there is no noise [40], and using the new gray the median degree value replaces the original noise points so that the algorithm can better retain the texture details of the image while filtering the noise.

4.2.2. Texture Feature Extraction of Defect Images. As a global feature, texture is a ubiquitous but difficult to describe possibility in images. The texture attribute refers to the law of change from pixel level to gray level in an image, which is an irregular but normal feature in the macroscopic view. We extracted the texture features of the cracks, holes, scratches, and inclusion defects in the samples, and the extraction results are shown in Table 3. We make a histogram based on this result, as shown in Figure 4.

It can be seen from Figure 4 that from the feature data extracted above, the difference between different features of different types or the same type is also very large. Because there is a unique sample, using this data for defect classification will cause the classifier to converge too late or even fail to converge, resulting in low classification accuracy or classification failure. Therefore, before classification, different methods should be selected according to needs. The exported attribute data has been standardized.

4.2.3. Standardized Processing of Characteristic Data. Here, our method is to standardize the extracted feature data. We choose the linear scale transformation method, the range transformation method, and the standard sample transformation method. These three methods are different. The standard values of the data after linear transformation are all in (within the range of 0, 1); when the positive and negative indicators are equalized to positive indicators, the optimal value is 1, the worst value is 0, and the larger the value, the better. When the maximum value of a positive indicator is 0, this method cannot be used to standardize the indicator; when the value of a reverse indicator is 0, this method cannot be used to standardize the indicator. The results are shown in Table 4. We make a radar chart based on this result, as shown in Figure 5.

It can be seen from Figure 5 that the values of the four indicators of the hole are all equal, so the standard sample transformation method and the range transformation method cannot be used, but the linear proportional transformation method can only be used; the values of the four indicators of the crack are all close to 0, so the range transformation method cannot be used and the linear scale transformation method can only use the standard sample transformation method; the values of the four indicators of abrasion are all close to 1; and you can choose to use the range transformation method and the linear proportional transformation method; the values are close to 1; you can choose to use the range transformation method and the linear scale transformation method.

4.3. Experimental Results Based on Image Denoising

4.3.1. Analyze according to Different Algorithm Experiments. Through four different strip steel surface defect detection system designs, work in the same environment at the same time to analyze the changes in detection accuracy. Data-type factors adopt independent sample *t*-test, and the experimental results are shown in Table 5. We make an area map based on this result, as shown in Figure 6.

Figure 6 shows that the median filter and Gaussian filter have a particularly poor effect on salt and pepper noise. The middle filter can remove the salt and pepper noise in the middle, but it is not effective at the edges of the salt and pepper noise. The intermediate filter based on partial differentiation has the effect of salt and pepper noise, which is better. As the concentration of salt and pepper noise increases, the average Gaussian filter and filter are less capable of handling salt and pepper noise. Medium filtering still does not perform well in terms of edge noise. The medium filter based on partial differential has the best effect on the noise of salt and pepper.

4.3.2. Analyze according to the Signal-to-Noise Ratio and Variance Value. In order to compare different filtering effects more intuitively, this article uses signal-to-noise ratio and variance to evaluate the image quality after skipping. Comparing the maximum signal-to-noise ratio and image fluctuation after denaturation under different salt and pepper noise concentrations, it can be compared that the filtering effect studied in this paper is the best. Through experiments, the maximum signal-to-noise ratio and change value of each filter under different salt and pepper noise concentrations are obtained, as shown in Figure 6. We make a line chart based on this result, as shown in Figure 7.

It can be seen from Figure 7 that after processing the mean filter and Gaussian filter images, the average MSE fluctuation value is relatively large, and as the salt and pepper noise concentration increases, the growth rate of MSE increases significantly, and the signal-to-noise ratio also increases with the average fluctuation value. The increase in MSE continues to decrease, and image distortion becomes more serious. After performing intermediate filtering and adaptive filtering on the image, compared with the first two images, the image distortion is reduced, but the distortion is also more serious. After filtering the image, the image repayment effect is better.

5. Conclusions

An effective threshold segmentation algorithm for coefficient of variation is proposed. This algorithm overcomes the disadvantage of using only one threshold per iteration in repeated threshold segmentation. It also utilizes the sliding window used in adaptive threshold segmentation, which reduces the amount of calculation and improves detection efficiency. The system structure of the whole system is designed, and the system is divided into imaging module, fault detection software module, and storage management module. According to different principles of detection methods, different image capturing methods are given. The overall process of defect detection software is designed, and the design and implementation of basic software units are introduced in detail. This paper analyzes the design of the steel strip surface defect detection system based on machine vision. According to the application requirements of machine vision technology, based on the surface quality of strip steel, the detection of surface defects is adjusted and optimized for the design of this article. Experiments prove that the method designed in this paper is very effective. We hope that the research in this article can provide a theoretical basis for the design method of steel surface defect detection system based on machine vision.

At present, most retinal blood vessel extraction methods are mainly used for normal retinal images. Therefore, when applied to a large range of lesion images, it is difficult to accurately extract blood vessels due to the interference of lesions and other nonvascular structures, and a large number of nonvascular structures cannot be filtered. In addition, this article focuses on vascular bone extraction and vascular structure segmentation methods suitable for retinal imaging. Analyze the characteristics of defects, and find the entry point for

detecting defects. According to the edge feature, uneven texture feature, and uneven defect feature, the defect detection method based on edge feature, the defect detection method based on unequal texture feature, and the defect detection method based on irregular feature are proposed. The techniques and theories on which this method relies are introduced and discussed.

The steel industry occupies an important position in China's economic industry. It can be regarded as the main core of manufacturing. This is an intensive industry that has accumulated a lot of capital and energy. Although China produces a large amount of steel every year, the quality of various steel products in China is obviously not as good as that of developed countries. In the quality of steel products, the importance of surface quality is self-evident, but improving quality is always difficult. Improving the surface quality of steel is of great significance to improving market competitiveness. Accurate detection of steel plate surface defects and the establishment of a steel plate surface defect evaluation system are important conditions for improving the quality of steel plates. This article makes full use of the image data of steel surface defects and introduces artificial intelligence methods to classify and identify steel defects and target detection. It solves the problem of long iteration time of ant colony optimization algorithm and particle optimization algorithm. The algorithm is easy to fall into local optimization, improves the classification accuracy of the support machine, optimizes the optimization process, and is made of steel.

Data Availability

The data underlying the results presented in the study are available within the manuscript.

Conflicts of Interest

The authors declare that they have no conflicts of interest.

References

[1] K. Shankar, Y. Zhang, Y. Liu, L. Wu, and C.-H. Chen, "Hyperparameter tuning deep learning for diabetic retinopathy fundus image classification," *IEEE Access*, vol. 8, pp. 118164–118173, 2020.

[2] Y. Tang, S. Fang, J. Chen, L. Ma, L. Li, and X. Wu, "Axial compression behavior of recycled-aggregate-concrete-filled GFRP-steel composite tube columns," *Engineering Structures*, vol. 216, article 110676, 2020.

[3] N. Gao and Y. Zhang, "A low frequency underwater metastructure composed by helix metal and viscoelastic damping rubber," *Journal of Vibration and Control*, vol. 25, no. 3, pp. 538–548, 2019.

[4] T. Ohkubo, N. Terada, and Y. Yoshida, "Preliminary scanning fluorescence detection of a minute particle running along a waveguide implemented microfluidic channel using a light switching mechanism," *Microsystem Technologies*, vol. 22, no. 6, pp. 1227–1240, 2016.

[5] J. Zhao, J. Huang, R. Wang, H. R. Peng, and S. Ji, "Investigation of the optimal parameters for the surface finish of k9 optical

glass using a soft abrasive rotary flow polishing process," *Journal of Manufacturing Processes*, vol. 49, pp. 26–34, 2020.

[6] S. Liu, Y. Sun, M. Gu, C. Liu, L. He, and Y. Kang, "Review and analysis of three representative electromagnetic NDT methods," *Insight-Non-Destructive Testing and Condition Monitoring*, vol. 59, no. 4, pp. 176–183, 2017.

[7] S. K. Choudhary, A. Kumar, S. Ganguly, M. Laru, and E. Z. Chacko, "Application of thermodynamics in mitigating wire rod chipping during hot rolling of continuously cast steel billets," *ISIJ International*, vol. 58, no. 10, pp. 1811–1819, 2018.

[8] M. P. Dombrowski, J. Labelle, D. G. McGaw, and M. C. Broughton, "An autonomous receiver/digital signal processor applied to ground-based and rocket-borne wave experiments," *Journal of Geophysical Research: Space Physics*, vol. 121, no. 7, pp. 7334–7343, 2016.

[9] S. B. Shu, C. M. Yu, C. Liu, M.-W. Chen, Y.-Z. Zhang, and X. Li, "Improved plasma position detection method in EAST Tokamak using fast CCD camera," *Nuclear Science and Techniques*, vol. 30, no. 2, pp. 67–76, 2019.

[10] M. A. Hossam, H. M. Ebied, M. H. Abdel-Aziz, and M. F. Tolba, "Accelerated hyperspectral image recursive hierarchical segmentation using GPUs, multicore CPUs, and hybrid CPU/GPU cluster," *Journal of Real-Time Image Processing*, vol. 14, no. 2, pp. 413–432, 2018.

[11] X. Q. Zhang and S. G. Zhao, "Cervical image classification based on image segmentation preprocessing and a CapsNet network model," *International Journal of Imaging Systems and Technology*, vol. 29, no. 1, pp. 19–28, 2019.

[12] C. Zuo, L. Jovanov, B. Goossens et al., "Image denoising using quadtree-based nonlocal means with locally adaptive principal component analysis," *IEEE Signal Processing Letters*, vol. 23, no. 4, pp. 434–438, 2016.

[13] L. Feng and L. Lin, "Comparative analysis of image denoising methods based on wavelet transform and threshold functions," *International Journal of Engineering Transactions B Applications*, vol. 30, no. 2, pp. 199–206, 2017.

[14] C. Yang, Z. Yang, and Z. Deng, "Robust weighted state fusion Kalman estimators for networked systems with mixed uncertainties," *Information Fusion*, vol. 45, pp. 246–265, 2019.

[15] K. J. H. Law, H. Tembine, and R. Tempone, "Deterministic mean-field ensemble Kalman filtering," *SIAM Journal on Scientific Computing*, vol. 38, no. 3, pp. A1251–A1279, 2016.

[16] M. V. Basin, "Root-mean-square filtering of the state of polynomial stochastic systems with multiplicative noise," *Automation & Remote Control*, vol. 77, no. 2, pp. 242–260, 2016.

[17] M. Elhoseny and K. Shankar, "Optimal bilateral filter and convolutional neural network based denoising method of medical image measurements," *Measurement*, vol. 143, pp. 125–135, 2019.

[18] R. K. Wang, C. R. Chatwin, and R. C. D. Young, "Assessment of a Wiener filter synthetic discriminant function for optical correlation," *Optics & Lasers in Engineering*, vol. 22, no. 1, pp. 33–51, 2016.

[19] M. L. Honig and J. S. Goldstein, "Adaptive reduced-rank interference suppression based on the multistage Wiener filter," *IEEE Transactions on Communications*, vol. 50, no. 6, pp. 986–994, 2016.

[20] J. Yang, Z. Yang, J. Liu, B. Jiang, W. Lu, and X. Gao, "No reference quality assessment for screen content images using stacked auto-encoders in pictorial and textual regions," *IEEE Transactions on Cybernetics*, pp. 1–13, 2020.

[21] Y. Li, J. Liu, and Y. Wang, "Railway wheel flat detection based on improved empirical mode decomposition," *Shock and Vibration*, vol. 2016, Article ID 4879283, 14 pages, 2016.

[22] E. Cauda, A. Miller, and P. Drake, "Promoting early exposure monitoring for respirable crystalline silica: taking the laboratory to the mine site," *Journal of Occupational & Environmental Hygiene*, vol. 13, no. 3, pp. D39–D45, 2016.

[23] S. Ren and F. Liu, "The optimal thresholding technique for image segmentation using fuzzy Otsu method," *Advances in Computational Sciences and Technology*, vol. 11, no. 6, pp. 445–454, 2018.

[24] Z. Luo, T. Wu, Z. He, and X. Chen, "Extraction of sea-clutter and RFI regions based on image segmentation for high-frequency sky-wave radar," *IET Radar, Sonar & Navigation*, vol. 13, no. 1, pp. 58–64, 2019.

[25] Y. Liu, C. Yang, and Q. Sun, "Thresholds based image extraction schemes in big data environment in intelligent traffic management," *IEEE Transactions on Intelligent Transportation Systems*, pp. 1–9, 2020.

[26] T. Sathiya and B. Sathiyabhama, "Fuzzy relevance vector machine based classification of lung nodules in computed tomography images," *International Journal of Imaging Systems and Technology*, vol. 29, no. 3, pp. 360–373, 2019.

[27] X. Wang, X. Zhao, Y. Zhu, and X. Su, "NSST and vector-valued C–V model based image segmentation algorithm," *IET Image Processing*, vol. 14, no. 8, pp. 1614–1620, 2020.

[28] S. Wan, Y. Xia, L. Qi, Y. H. Yang, and M. Atiquzzaman, "Automated colorization of a grayscale image with seed points propagation," *IEEE Transactions on Multimedia*, vol. 22, no. 7, pp. 1756–1768, 2020.

[29] J. Qin, X. Shen, F. Mei, and Z. Fang, "An Otsu multi-thresholds segmentation algorithm based on improved ACO," *The Journal of Supercomputing*, vol. 75, no. 2, pp. 955–967, 2019.

[30] Y. Liu, Y. Chen, B. Han, Y. Zhang, X. Zhang, and Y. Su, "Fully automatic breast ultrasound image segmentation based on fuzzy cellular automata framework," *Biomedical Signal Processing & Control*, vol. 40, pp. 433–442, 2018.

[31] H. Chen, D. Fan, J. Huang, W. Huang, G. Zhang, and L. Huang, "Finite element analysis model on ultrasonic phased array technique for material defect time of flight diffraction detection," *Science of Advanced Materials*, vol. 12, no. 5, pp. 665–675, 2020.

[32] X. Deng, Y. Du, C. Wang, and X. Wang, "An adaptive threshold corner detection algorithm based on auto-correlation matrix of image pixel," *Transactions of the Chinese Society of Agricultural Engineering*, vol. 33, no. 18, pp. 134–140, 2017.

[33] Y. Sun, "Analysis for center deviation of circular target under perspective projection," *Engineering Computations*, vol. 36, no. 7, pp. 2403–2413, 2019.

[34] C.-y. Han, "Improved SLIC imagine segmentation algorithm based on K-means," *Cluster Computing*, vol. 20, no. 2, pp. 1–7, 2017.

[35] Z. Wang, Y. Wang, L. Jiang, C. Zhang, and P. Wang, "An image segmentation method using automatic threshold based on improved genetic selecting algorithm," *Automatic Control and Computer Sciences*, vol. 50, no. 6, pp. 432–440, 2016.

[36] L. Sun, Y. Li, Y. Zou, and Y. Li, "Pig image segmentation method based on improved graph cut algorithm," *Transactions of the Chinese Society of Agricultural Engineering*, vol. 33, no. 16, pp. 196–202, 2017.

[37] F. Argüello, D. L. Vilariño, D. B. Heras, and A. Nieto, "GPU-based segmentation of retinal blood vessels," *Journal of Real-Time Image Processing*, vol. 14, no. 4, pp. 773–782, 2018.

[38] N. Krishnaraj, M. Elhoseny, M. Thenmozhi, M. M. Selim, and K. Shankar, "Deep learning model for real-time image compression in Internet of Underwater Things (IoUT)," *Journal of Real-Time Image Processing*, vol. 17, no. 6, pp. 2097–2111, 2020.

[39] F. Xiao, "Multi-sensor data fusion based on the belief divergence measure of evidences and the belief entropy," *Information Fusion*, vol. 46, pp. 23–32, 2019.

[40] L. Zhang, H.-M. Shi, X.-H. Zeng, and Z. Zhuang, "Theoretical and experimental study on the transmission loss of a side outlet muffler," *Shock and Vibration*, vol. 2020, Article ID 6927574, 8 pages, 2020.